Speed Response Analysis of Servo Motor and Control Strategy for Fast Transient Response

Cheolmin Hwang[1], Gyu Cheol Lim, Sangwon Lee, and Jung-Ik Ha[2]
Electrical and Computer Engineering Department, Seoul National University, Seoul, South Korea
E-mail: {wj1520[1],jungikha[2]}@snu.ac.kr

***Abstract*-- This paper presents an analysis of the speed transient performance of a servo motor, including their physical limit and a nominal speed response frequency. A new indicator of transient performance for servo drives is also introduced, which is obtained from the measured speed response frequency using a proposed scaling method. This method reduces the dependency on changes in speed reference in case of step response analysis. The proposed transient performance indicator is the ratio of this scaled value to the nominal speed response frequency, which reflects how close the servo drive's transient performance is to the limit transient performance of the servo motor. This paper also proposes the control strategy to fully utilize the physical limit of the speed transient performance. A strategy includes the predictive current control with finite-control-set to utilize the maximum output voltage, as well as a criterion for smooth transition of the current to the steady state. Additionally, the torque feedforward method is proposed to achieve the fast transient response of speed. The proposed control strategy is verified by experimental results and analyzed by the new transient performance indicator.**

***Index Terms*—Speed response, transient performance, torque feedforward, predictive current control.**

I. INTRODUCTION

Servo drive systems are widely used in various applications, such as automated machines, machine tools, and wearable robots, where precise operation is required. To achieve accurate and responsive operation, fast transient response of speed and current is essential for servo drives. Various control strategies for fast transient response have been studied [1]–[5]. However, there was lack of analysis of the servo motors' transient performance limits and servo drives' transient performance specifications. It is necessary to investigate the unclearness of the speed response analysis.

Some servo drive manufacturers use steady state analysis to represent the transient performance of their products by applying a sinusoidal speed reference. However, it is challenging to generate a sinusoidal speed reference of several kHz or more [6], and the criterion for determining the reference magnitude needs to be clarified. In addition, considering the actual operation of servo motors, it is more appropriate to use a transient analysis applying a step reference to evaluate a quantitative performance specification. In step response analysis, physical quantities with units of time or frequency are used as quantitative indicators representing the transient performance. However, these values have a dependency on the step reference magnitude. A smaller magnitude of the step reference converges the control variable faster, whereas a larger magnitude of the step reference slows down the convergence rate and is determined dominantly by the current limit and the inertia of the system.

This paper presents an analysis of the ideal speed response frequency ($f_{\omega,ideal}$), which represents the physical limit of servo motors' transient performance in assumption of the ideal torque and voltage waveforms for fast convergence. $f_{\omega,ideal}$ is evaluated by system variables of the target servo system with variations of the speed reference change ($\Delta\omega_m^*$). In addition, the indicator of servo drives' transient performance, which represents how close the speed response frequency (f_ω) of the servo drive is to $f_{\omega,ideal}$, is proposed using a scaling method. This scaling method reduces the dependency of the measured f_ω on $\Delta\omega_m^*$.

The other part of this paper is related to the control strategy for fast transient performance. For fast transient performance, direct torque control (DTC) was proposed [7]. DTC directly outputs an active voltage vector during a whole sampling interval from the torque reference based on estimated flux linkage and torque. DTC is suitable for the application requiring fast transient performance, but it has a tradeoff that the steady state current ripple is more significant than that of field oriented control (FOC) [8]. This tradeoff can cause a current overshoot in the transient state. [9] introduced duty-ratio based DTC (DDTC), and [10] adopted a variable sampling frequency method to prevent the current overshoot. However, these papers focused on the transient performance of current rather than the speed.

Model predictive control (MPC) has been presented recently due to its simple implementation, various objectives for the cost function, and easy considering of nonlinearities [11], [12]. Finite-control-set MPC (FCS-MPC) outputs a voltage vector minimizing a cost function among seven voltage vectors, so it has been compared to DTC. [13] presented the model predictive direct speed control (MP-DSC), which has the speed error term as the objective of the cost function. Although speed reference tracking is implemented in a simple structure, the voltage margin cannot be fully utilized since only adjacent or zero voltage vectors are used to reduce the current ripple and the number of switching.

This paper proposes the control strategy for fast transient performance, which includes two parts, current control part and speed control part. The current control part

adopts the finite-control-set predictive current control (FCS-PCC) to utilize the maximum output voltage under transient conditions. The transition method to FOC is introduced to prevent the current overshoot. The speed control part presents the torque feedforward method for the ideal torque waveform shaping. For the speed to converge fast without overshoot, it is crucial to implement the exact voltage reversal instant since the sign of voltage determines whether the current increases or decreases. Finally, the transient performance of servo drives, the result of the proposed control strategy is expressed by the proposed transient performance indicator, which is experimentally verified by comparing it with results of the conventional cascaded PI control.

II. Analysis of the Speed Response Frequency

Several specifications indicate the transient performance of the step response, such as a time constant, a rise time, and a settling time. Among them, the rise time t_r, defined as a time interval when the response changes from 10% to 90%, is adopted to calculate f_ω in this paper due to its ease of measurement. f_ω based on the rise time is defined by

$$f_\omega \equiv \frac{1}{\tau} = \frac{2.2}{t_{90}-t_{10}} = \frac{2.75K_t}{J\Delta\omega_m^*}\langle i_{qs}^r\rangle_{(t_{10},t_{90})} \tag{1}$$

where τ is the time constant of the speed response, K_t is the torque constant, J is the inertia of the system, i_{qs}^r is the q-axis stator current, the superscript "r" represents the synchronous reference frame, and $\langle\cdot\rangle_{(a,b)}$ represents an average value from $t=a$ to $t=b$. t_{10} and t_{90} are the times when changes of the speed response reach 10% and 90% $\Delta\omega_m^*$, respectively. The relationship between τ and $t_r = t_{90}-t_{10}$ in the first-order system is used [14]. K_t/J is determined by the system configuration, $\Delta\omega_m^*$ is the input of the speed controller, and the average current is determined by the transient performance of the speed controller.

Equation (1) is derived from a mechanical equation of the servo system

$$\frac{d\omega_m}{dt} = \frac{1}{J}(T_e - T_l - B\omega_m) \tag{2}$$

where ω_m is the mechanical rotating speed, T_e is the output torque, T_l is the load torque, and B is the viscous friction coefficient.

The time response of speed is derived as

$$\omega_m(t) = e^{-\frac{B}{J}t}\left(\omega_{m0} + \int_0^t e^{\frac{B}{J}\tau}\frac{T_e - T_l}{J}d\tau\right) \tag{3}$$

where ω_{m0} is the initial value of ω_m when $\Delta\omega_m^*$ is recognized. The change of the speed response from t_{10} to t_{90} is derived as

$$\omega_{m90} - \omega_{m10} = 0.8\Delta\omega_m^* \cong \int_{t_{10}}^{t_{90}}\frac{K_t i_{qs}^r}{J}d\tau \tag{4}$$

where $\omega_{m10} = \omega_m(t_{10})$ and $\omega_{m90} = \omega_m(t_{90})$. In this paper, the target motor is a surface-mounted permanent magnet synchronous machine (SMPMSM) with a torque equation

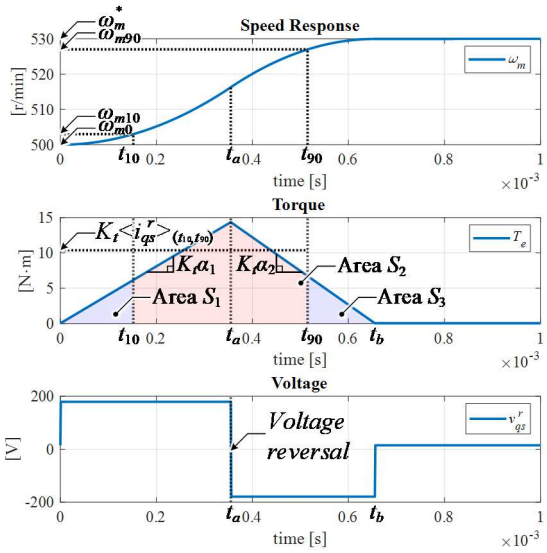

Fig. 1 An example of speed response, torque, and voltage waveforms in the ideal case.

$$T_e = \frac{3}{2}\frac{P}{2}\lambda_f i_{qs}^r = K_t i_{qs}^r \tag{5}$$

where P is the number of poles, and λ_f is the flux linkage of a permanent magnet. It is assumed that $e^{(B/J)t} \cong 1$ because it deals with speed changes over a short period. Also, it is assumed that T_l is included in the friction torque.

A. Ideal Speed Response Frequency

It is seen from (1) that the transient performance is proportional to the average current. It is necessary to consider limiting factors of f_ω to analyze the ideal case of fast transient performance. The first limiting factor is the voltage applied to the stator since the time derivative of i_{qs}^r is determined as

$$\frac{di_{qs}^r}{dt} = \frac{v_{qs}^r - R_s i_{qs}^r - e_{qs}^r}{L_s} \tag{6}$$

where v_{qs}^r is the q-axis stator voltage, R_s is the stator resistance, L_s is the stator inductance, and $e_{qs}^r = \omega_r\lambda_f$ is the q-axis back electromotive force (EMF).

Considering the limiting factor of the voltage, the positive and negative i_{qs}^r slopes of α_1 and α_2, respectively, are set to constant and maximum values as

$$\begin{aligned}\alpha_1 &= (2/3V_{dc} - \omega_{r0}\lambda_f)/(2/3L_s),\\ \alpha_2 &= (-2/3V_{dc} - \omega_{r0}\lambda_f)/(2/3L_s)\end{aligned} \tag{7}$$

where V_{dc} is a DC link voltage. The maximum applied voltage and the saturated inductance are assumed to be $2/3V_{dc}$ and $2/3L_s$, respectively. e_{qs}^r is assumed to stay at its initial value $\omega_{r0}\lambda_f$, where ω_{r0} is the initial value of ω_r.

Fig. 1 shows the ideal case of the speed response, the torque, and the voltage waveforms in the acceleration operation. Since the current slopes are assumed to be

constant, the ideal value of f_ω is obtained using the triangle area equations as follows:

$$S_1 = 0.5K_t|\alpha_1|t_{10}^2 = 0.1J\Delta\omega_m^* \tag{8}$$

$$S_3 = 0.5|\alpha_2|K_t(t_b - t_{90})^2 = 0.1J\Delta\omega_m^* \tag{9}$$

$$S_1 + S_2 + S_3 = 0.5K_t|\alpha_1|t_a t_b = J\Delta\omega_m^* \tag{10}$$

where t_a is the voltage reversal time and t_b is the convergence time. Thus, the ideal speed response frequency is derived as

$$f_{\omega,ideal}^{VL} = \frac{2.2}{\left(\sqrt{\frac{2|\alpha_1 - \alpha_2|}{|\alpha_1\alpha_2|}} - \sqrt{\frac{0.2}{|\alpha_1|}} - \sqrt{\frac{0.2}{|\alpha_2|}}\right)\sqrt{\frac{J\Delta\omega_m^*}{K_t}}} \tag{11}$$

using (8)-(10), and the relationship between t_a and t_b

$$(\alpha_1 - \alpha_2)t_a + \alpha_2 t_b = 0. \tag{12}$$

The superscript "VL", which means the voltage limit, represents that the voltage magnitude is always the maximum allowable value for the maximum current slopes. Since the current slopes are set to the instantaneous maximum slopes, as shown in (7), (11) represents the physical limit of the servo motor's transient performance.

On the other hand, the second limiting factor, the current limit comes into play when $\Delta\omega_m^*$ exceeds a specific value. When the peak value of the q-axis stator current in the voltage limit condition described as

$$i_{qs,peak}^{r,VL} = \alpha_1 t_a = \sqrt{\frac{|\alpha_1\alpha_2|}{|\alpha_1 - \alpha_2|}\frac{2J\Delta\omega_m^*}{K_t}} \tag{13}$$

reaches the maximum instantaneous value of current, the torque waveform becomes trapezoidal due to the current limit. This value of the speed reference change is defined as the nominal speed reference change $\Delta\omega_{m,nom}^*$, and it is evaluated as

$$\Delta\omega_{m,nom}^* = \frac{9}{2}\frac{K_t}{J}\frac{|\alpha_1 - \alpha_2|}{|\alpha_1\alpha_2|}I_{rated}^2 \tag{14}$$

where I_{rated} is the rated current. Most catalogues of manufacturers provide the rated torque $T_{e,rated} = K_t I_{rated}$ as a continuous rating and 2~3 times $T_{e,rated}$ as a maximum instantaneous torque. Therefore, the maximum instantaneous current is set to $3I_{rated}$ in this analysis. The maximum instantaneous current refers to the highest level of current that the motor can safely handle for one second without overheating.

In conclusion, Fig. 2 shows the transient performance limited either by the applied voltage or by the current-handling capability of the system. When $\Delta\omega_m^*$ is smaller than $\Delta\omega_{m,nom}^*$, the system is in the voltage limit region, where the voltage magnitude becomes the limiting factor. In contrast, when $\Delta\omega_m^*$ exceeds $\Delta\omega_{m,nom}^*$, the system operates in the region defined as the current limit region, where the current-handling capability becomes the limiting factor. The ideal speed response frequency in the current limit region is calculated as

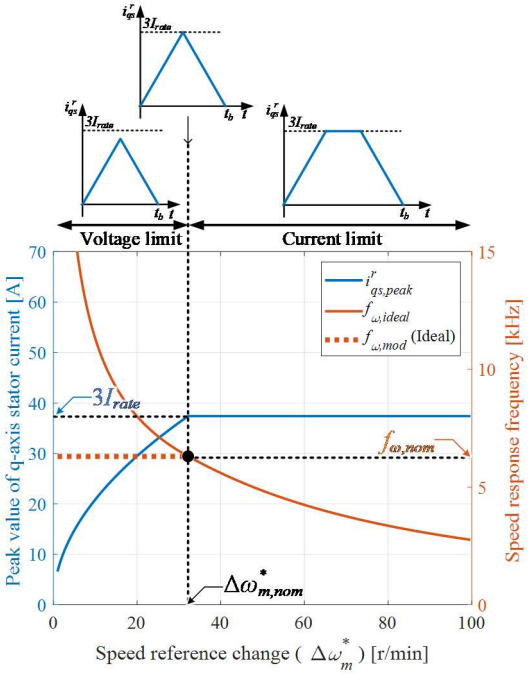

Fig. 2 Speed response frequency and the peak value of q-axis stator current with the speed reference change variation.

$$f_{\omega,ideal}^{CL} = \frac{2.2}{\frac{J\Delta\omega_m^*}{3K_t I_{rated}} - \frac{3I_{rated}}{2}\left(\frac{1}{|\alpha_1|} + \frac{1}{|\alpha_2|}\right) - \sqrt{\frac{J\Delta\omega_m^*}{5K_t}}\left(\frac{1}{\sqrt{|\alpha_1|}} + \frac{1}{\sqrt{|\alpha_2|}}\right)} \tag{15}$$

in a similar manner to $f_{\omega,ideal}^{VL}$ derivation. In this case, it is assumed that $i_{qs}^r(t)\big|_{t_{10}} < 3I_{rated}$ and $i_{qs}^r(t)\big|_{t_{90}} < 3I_{rated}$. Then, the final ideal speed response frequency $f_{\omega,ideal}$ is defined as

$$f_{\omega,ideal} = \begin{cases} f_{\omega,ideal}^{VL} & (\Delta\omega_m^* < \Delta\omega_{m,nom}^*) \\ f_{\omega,ideal}^{CL} & (\Delta\omega_m^* > \Delta\omega_{m,nom}^*) \end{cases}. \tag{16}$$

B. Proposed Nominal Speed Response Frequency and Transient Performance Indicator

$f_{\omega,ideal}$ described in (16) is difficult to be the most appropriate indicator of servo motors' transient performance since it varies with respect to the $\Delta\omega_m^*$ as shown in Fig. 2. Therefore, the ideal speed response frequency at $\Delta\omega_m^* = \Delta\omega_{m,nom}^*$ is defined as the nominal speed response frequency $f_{\omega,nom}$ and used as a representative value indicating the transient performance limit of servo motors. $f_{\omega,nom}$ is derived as

$$f_{\omega,nom} = \frac{2.2}{\left(\frac{3|\alpha_1 - \alpha_2|}{|\alpha_1\alpha_2|} - \sqrt{|\alpha_1 - \alpha_2|}\left(\sqrt{\frac{0.9}{|\alpha_1|}} - \sqrt{\frac{0.9}{|\alpha_2|}}\right)\right)I_{rated}} \tag{17}$$

by substituting (14) into $\Delta\omega_m^*$ of (11).

The measured f_ω needs to be scaled to reduce the dependency on $\Delta\omega_m^*$ to evaluate the transient performance of servo drives. It also needs to have the unit of hertz to be compared with $f_{\omega,nom}$.

The proposed scaling method is presented in

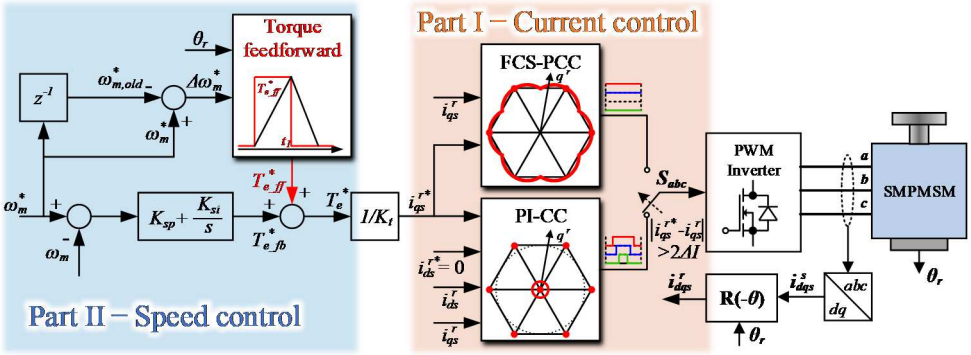

Fig. 3 Proposed control strategy: part 1 – transition method from PCC to PI-CC, part 2 – torque feedforward method.

$$f_{\omega,mod} \equiv f_{\omega} \frac{\Delta\omega_m^*}{i_{qs,peak}^r} \frac{i_{qs,peak}^r\big|_{\Delta\omega_m^*=\Delta\omega_{m,nom}^*}}{\Delta\omega_{m,nom}^*} \quad (18)$$
$$\left(\Delta\omega_m^* \in \left(0, \Delta\omega_{m,nom}^*\right)\right).$$

In the voltage limit region of ideal case, $f_{\omega} = f_{\omega,ideal}^{VL}$ and $i_{qs,peak}^r = i_{qs,peak}^{r,VL}$. The first multiplier $\Delta\omega_m^*/i_{qs,peak}^r$ makes f_{ω} independent on $\Delta\omega_m^*$, since $f_{\omega,ideal}^{VL}$ is inversely proportional to $\sqrt{\Delta\omega_m^*}$ and $i_{qs,peak}^{r,VL}$ is proportional to $\sqrt{\Delta\omega_m^*}$. The other multiplier makes $f_{\omega,mod}\big|_{\Delta\omega_m^*=\Delta\omega_{m,nom}^*}$ equal to $f_{\omega}\big|_{\Delta\omega_m^*=\Delta\omega_{m,nom}^*}$. In other words, $f_{\omega,mod}$ is normalized based on f_{ω} when $\Delta\omega_m^*$ is equal to $\Delta\omega_{m,nom}^*$. Specifically, $i_{qs,peak}^r\big|_{\Delta\omega_m^*=\Delta\omega_{m,nom}^*} = 3I_{rated}$ and $f_{\omega,mod} = f_{\omega,nom}$ in the voltage limit region of ideal case as shown in Fig. 2. Since $f_{\omega,mod}$ is constant when $\Delta\omega_m^*$ varies in the voltage limit region, the modified speed response frequency $f_{\omega,mod}$, which is the result of the scaling method, is defined in the voltage limit region. Therefore, the performance indicator of servo drives for fast transient performance is defined as

$$\gamma = f_{\omega,mod}/f_{\omega,nom} \quad (19)$$

A value of γ, which is equal to 1, represents the corresponding servo drive has the ideal performance. The servo drives with γ value closer to 1 have better transient performance.

III. Control Strategy for The Fast Transient Response

The proposed control strategy to approach the ideal waveform shown in Fig. 1 is depicted in Fig. 3, which consists of two main parts: current control and speed control. In the current control part, PCC is used to provide the maximum voltage in the transient state, while proportional-integral current control (PI-CC) is applied to prevent overshoot and reduce ripple in steady state. In the speed control part, a feedforward torque reference $T_{e,ff}^*$ is generated during the period of the calculated voltage reversal time t_1. $T_{e,ff}^*$ and t_1 are obtained considering triangular torque waveform and $\Delta\omega_m^*$.

A. Control Strategy Part I - Current Control

FCS-PCC outputs the full duty ratio (0 or 1) in carrier-based pulse width modulation (PWM), so it is effective for the transient state requiring a large voltage magnitude. However, it causes a significant ripple in the steady state due to small current errors. The transition method to PI-CC is adopted to reduce ripple components in the steady state.

Since completely achieving the ideal discontinuous voltage waveform in Fig. 1 is impossible in a digital control environment, it is crucial to determine the transition instant between PCC and PI-CC. This transition instant is based on the current error magnitude for convergence with small overshoots, as shown in the current control block diagram in Fig. 3. In other words, PCC is applied if the current error magnitude is greater than $2\Delta I$ considering the PWM delay. Otherwise, PI-CC is used. Once convergence is achieved, the output of the PI-CC deals only with the back EMF component. ΔI, which is set to

$$\Delta I = \left(2/3V_{dc} - R_s i_{qs}^r - \omega_r \lambda_f\right) T_s/L_s \quad (20)$$

represents the maximum magnitude of the current change during a sampling period T_s. The discrete-time equation is derived as

$$i_{qs}^r(k+1) = \left(1 - \frac{R_s T_s}{L_s}\right) i_{qs}^r(k) - T_s\omega_r\left(i_{ds}^r(k) + \frac{\lambda_f}{L_s}\right) + \frac{T_s}{L_s} v_{qs}^r \quad (21)$$

from (6) using the Euler method to apply PCC in the transient state [12]. The voltage vector that minimizes the cost function (22) among the seven voltage vectors is applied during a whole sampling interval based on the prediction model (21).

$$g = \left(i_{qs}^{r\,*} - i_{qs}^r(k+1)\right)^2 \quad (22)$$

As (22) has the only objective of the torque current reference tracking, the magnitude of q-axis stator voltage in the synchronous reference frame $\left|v_{qs}^r\right|$ varies with respect to the electrical rotor angle, as shown in Fig. 4(a).

B. *Control Strategy Part* II - *Speed Control*

Fig. 5 illustrates the key concept of the proposed control strategy for achieving fast transient performance. In contrast to the previous analyses, actual current slopes are not constant and depend on the current magnitude due to the inductance saturation and voltage drops across resistive elements, as shown in T_e waveform. The main goal is calculating $T_{e,ff}^*$ and t_1, for which T_e recovers the given $\Delta\omega_m^*$. $T_{e,calc}$ with constant current slopes, which has the same integral value as the integral of T_e, is used for calculating $T_{e,ff}^*$ and t_1.

Algorithm I represents the procedure for calculating $T_{e,ff}^*$ and t_1. It is conducted during only one sampling interval when $\Delta\omega_m^*$ is recognized. The voltage reversal instant is determined by the ratio of the current integrals in the rising interval and the falling interval. As shown in Fig. 5, since $T_{e,calc}$ is assumed to be a triangular waveform, this ratio is determined by rising and falling slopes of the current. The current slopes are determined by the output voltage, the resistive voltage drop, back EMF, and the inductance. Since inductance saturation is determined by the magnitude of the current, it has the same effect on the current slopes in each interval. Meanwhile, the output voltage varies with respect to the electrical rotor angle, and resistive voltage drops have an opposite effect on the current slopes of rising and falling interval. Therefore, the double calculation method is used, which is explained by following steps.

The step 1 approximately calculates t_1 by

$$t_1 = \sqrt{J\Delta\omega_m^* L_s \frac{\left(\overline{v_{qs}^r} + \overline{e_{qs}^r}\right)}{K_t \overline{v_{qs}^r}\left(\overline{v_{qs}^r} - \overline{e_{qs}^r}\right)}}, \tag{23}$$

which is derived using (10) and (12). In this step, α_1 and α_2 are set to $\left(\overline{v_{qs}^r} - \overline{e_{qs}^r}\right)/L_s$ and $\left(-\overline{v_{qs}^r} - \overline{e_{qs}^r}\right)/L_s$, where $\overline{v_{qs}^r} = 2/3V_{dc}$ and $\overline{e_{qs}^r} = \omega_{r0}\lambda_f$. Each variable is expressed using $\bar{(\cdot)}$, which represents a positive representative constant value. Then, t_2 is calculated using (12).

Step 2 updates representative values using average values. $\overline{i_{qs}^r}$ is calculated as

$$\overline{i_{qs}^r} = 0.5\left(\overline{v_{qs,p}^r} - \overline{e_{qs}^r}\right)t_1/L_s \tag{26}$$

to compensate resistive voltage drops using t_1 obtained from (23). In PCC, v_{qs}^r is a varying value with respect to the electrical rotor angle, and it is the periodic value with a 60 deg period. $\overline{v_{qs,p}^r}$ and $\overline{v_{qs,n}^r}$, which denote $\overline{v_{qs}^r}$ when v_{qs}^r is positive and negative, are calculated by (24). Fig. 4(b) shows two cases for calculating $\overline{v_{qs,p}^r}$ and $\overline{v_{qs,n}^r}$. To distinguish these cases, the initial electrical rotor angle

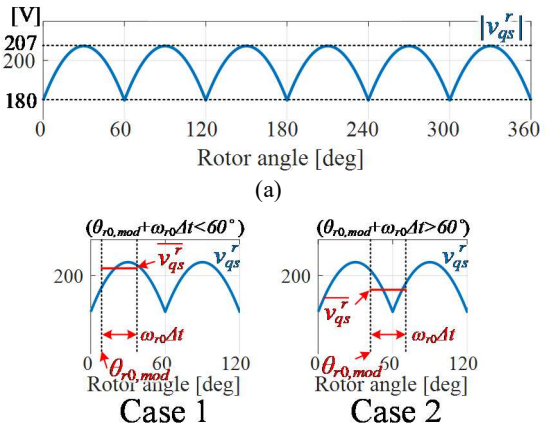

Fig. 4 (a) The change of $|v_{qs}^r|$ according to the electrical rotor angle and (b) the calculation of $\overline{v_{qs}^r}$.

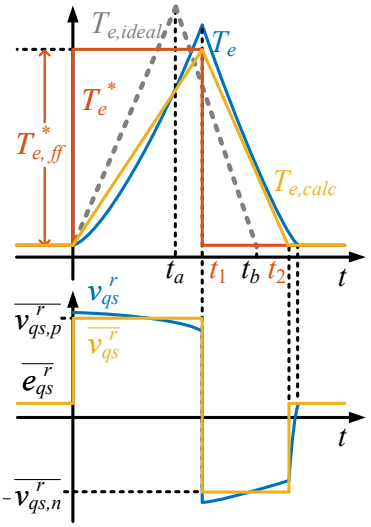

Fig. 5 Conceptual waveforms for the fast transient response.

ALGORITHM I. CONTROLLER ALGORITHM

Step 0	$\Delta\omega_m^*$ is recognized.
Step 1	Calculate t_1 and t_2 by (23) and (12).
Step 2	Update Representative values by (26) and (24).
Step 3	Calculate t_1 and $T_{e,ff}^*$ by (25).

θ_{r0} is modified to $\theta_{r0,mod} = \left(\theta_{r0} \bmod \pi/3\right)$. After the time interval Δt, if $\theta_{r0,mod} + \omega_{r0}\Delta t$ is less than $\pi/3$, it is case 1, and if it is larger, it is case 2. For example, in the calculation of $\overline{v_{qs,p}^r}$, $\Delta t = t_1$. On the other hand, in the calculation of $\overline{v_{qs,n}^r}$, $\Delta t = t_2 - t_1$, and $\theta_{r0,mod}$ is

$$\overline{v_{qs}^r} = \begin{cases} \dfrac{2/3V_{dc}}{\omega_{r0}\Delta t}\left(\sin\left(\theta_{r0,mod} + \omega_{r0}\Delta t - \dfrac{\pi}{6}\right) - \sin\left(\theta_{r0,mod} - \dfrac{\pi}{6}\right)\right) & \left(\theta_{r0,mod} + \omega_{r0}\Delta t < \dfrac{\pi}{3}\right) \\ \dfrac{2/3V_{dc}}{\omega_{r0}\Delta t}\left(1 - \sin\left(\theta_{r0,mod} - \dfrac{\pi}{6}\right) - \cos\left(\theta_{r0,mod} + \omega_{r0}\Delta t\right)\right) & \left(\theta_{r0,mod} + \omega_{r0}\Delta t > \dfrac{\pi}{3}\right) \end{cases} \tag{24}$$

$$t_1 = \sqrt{J\Delta\omega_m^* L_s \frac{\overline{v_{qs,n}^r} + R_s\overline{i_{qs}^r} + \overline{e_{qs}^r}}{0.5K_t\left(\overline{v_{qs,p}^r} + \overline{v_{qs,n}^r}\right)\left(\overline{v_{qs,p}^r} - R_s\overline{i_{qs}^r} - \overline{e_{qs}^r}\right)}}, \quad T_{e,ff}^* = K_t\frac{\overline{v_{qs}^r} - R_s\overline{i_{qs}^r} - \overline{e_{qs}^r}}{L_s}t_1 \tag{25}$$

replaced by $\left((\theta_{r0,mod} + \omega_{r0} t_1) \bmod \pi/3\right)$.

Step 3 calculates final $T^*_{e,ff}$ and t_1 by (25) using prior representative values. The compensation by $\overline{v^r_{qs}}$ and $\overline{i^r_{qs}}$ improves the accuracy of calculating t_1. Accurate calculations of $T^*_{e,ff}$ and t_1 are important for fast convergence without overshooting. However, due to the limitation of digital control, the actual voltage reversal instant has an error with t_1. Since PCC leads to maximum current slopes at the instant of t_1, the effect of this implementation error is even greater. Therefore, the proposed algorithm requires a high sampling frequency of at least 30 kHz.

IV. Experimental Verification

The motor parameters and experimental variables are listed in Table I. Fig. 6 shows the comparison of experimental results between the proposed method and the cascaded PI control method when $\omega_{m0} = 500$ r/min. The bandwidths of the cascaded speed and current PI controller are set to 100 Hz and 2 kHz respectively. These are maximum values that do not cause significant steady state ripple and overshoots. The key differences between two control methods are the voltage magnitude and the voltage reversal instant. The proposed control strategy maintains the voltage magnitude greater than $V_{dc}/\sqrt{3}$, which is the maximum output voltage under the linear modulation condition as shown in Fig. 6(a). On the other hand, as the output of cascaded PI control method is determined by the error between the reference value and the measured value, Fig. 6(b) cannot maintain its maximum voltage magnitude $V_{dc}/\sqrt{3}$ due to the decreasing current error. In addition, Fig. 6(a) has the discontinuous voltage waveform close to the ideal voltage waveform due to the pulsed shape of $T^*_{e,ff}$.

Fig. 7 shows the speed response and q-axis stator current waveforms of the target servo motor when $\Delta\omega^*_m$ varies from 5 r/min to $\Delta\omega^*_{m,nom} = 32.2$ r/min. As $\Delta\omega^*_m$ increases, the peak value of current also increases, and nonlinearity of current waveforms increases due to inductance saturation. It is shown that the peak value of current when $\Delta\omega^*_m$ is equal to $\Delta\omega^*_{m,nom}$, is smaller than $3I_{rate}$ as expected from Fig. 5. The convergence time of the cascaded PI control method is consistent with the variation of $\Delta\omega^*_m$ since outputs of controllers are determined based on the magnitude of error.

Fig. 8(a) shows the measured f_ω of each method. These results are obtained from each data set in Fig. 7. It shows that the proposed method has higher f_ω at all test points compared to the cascaded PI control method. When $\Delta\omega^*_m$ decreases from $\Delta\omega^*_{m,nom}$, f_ω increases for the proposed method, whereas for the cascaded PI control method, it does not increase. $f_{\omega,mod}$ derived from (18) has low dependency on $\Delta\omega^*_m$. This result suggests that for all $\Delta\omega^*_m < \Delta\omega^*_{m,nom}$, γ is used as the transient performance indicator as shown in Fig. 8(b). It is seen that $\langle\gamma\rangle = 0.933$ of the proposed method is much closer to the ideal $\gamma = 1$ than $\langle\gamma\rangle = 0.270$ of the cascaded PI control method, where $\langle\cdot\rangle$ represents the average value. As a

TABLE I.

MOTOR PARAMETERS AND EXPERIMENTAL VARIABLES

Parameters	Values
I_{rated}	12.4 A
ω_{base}	3000 r/min
Number of poles	8 poles
R_s	0.213 Ω
L_s	2.61 mH
λ_f	0.0713 V/(rad/s)
J	1.379×10^{-3} kgm^2
$sampling\ frequency$	30 kHz
V_{dc}	310 V

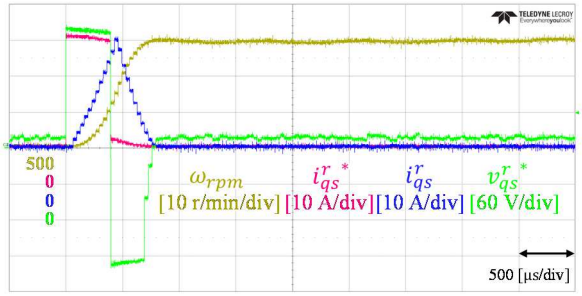

(a)

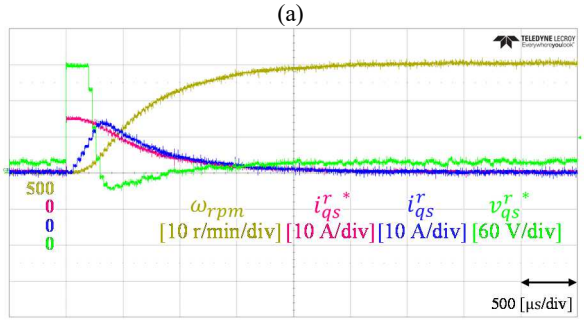

(b)

Fig. 6 Speed response of (a) proposed control strategy and (b) cascaded PI control when $\Delta\omega^*_m = 30$ r/min.

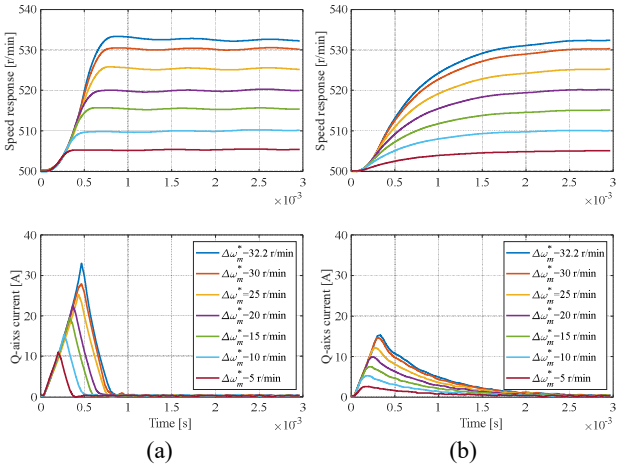

(a) (b)

Fig. 7 Speed response of (a) proposed control strategy and (b) cascaded PI control from $\Delta\omega^*_m = 5$ r/min to $\Delta\omega^*_m = \Delta\omega^*_{m,nom}$.

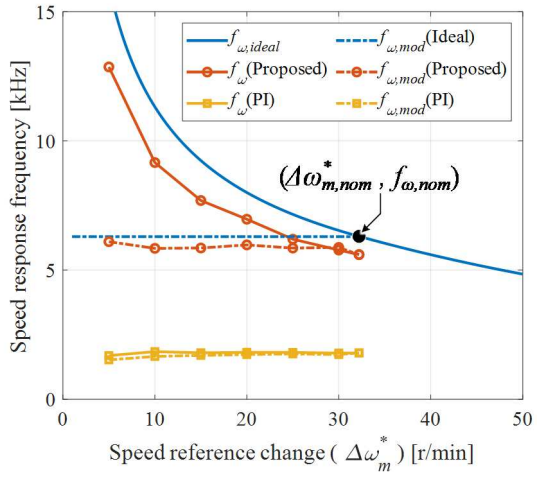

(a)

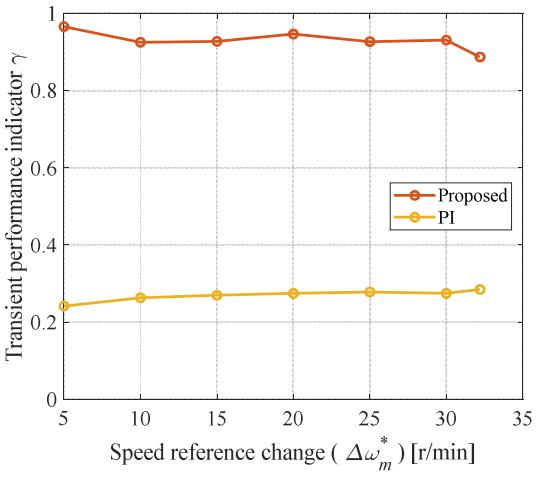

(b)

Fig. 8 (a) Analysis of the speed response frequency and (b) comparison of the transient performance specification γ.

result, the transient performance of the proposed control strategy is verified by the proposed transient performance indicator.

V. Conclusions

This paper proposed a new definition of a servo motor's nominal speed response frequency as a physical limit of the transient performance by analyzing the ideal speed response. The servo drive's transient performance indicator, which has low dependency on speed reference change, was also presented. This indicator represents how close the transient performance of the servo drive is to the maximum transient performance of the servo motor. In addition, the control strategy, including PCC and torque feedforward method for fast transient performance, was proposed. The maximum voltage magnitude larger than that of the linear modulation condition is guaranteed by PCC. The torque feedforward method makes the voltage waveform ideal discontinuous voltage waveform approximately. Finally, the proposed method better utilize the margins of voltage and current limits to approach the ideal response. The transient performance was verified by experimental results and compared to the conventional cascaded PI control method.

References

[1] X. Jiao, J. Zhang, and T. Shen, "An Adaptive Servo Control Strategy for Automotive Electronic Throttle and Experimental Validation," *IEEE Transactions on Industrial Electronics*, vol. 61, no. 11, pp. 6275–6284, Nov. 2014, doi: 10.1109/TIE.2014.2311398.

[2] M. H. Vafaie, B. Mirzaeian Dehkordi, P. Moallem, and A. Kiyoumarsi, "Minimizing Torque and Flux Ripples and Improving Dynamic Response of PMSM Using a Voltage Vector With Optimal Parameters," *IEEE Transactions on Industrial Electronics*, vol. 63, no. 6, pp. 3876–3888, Jun. 2016, doi: 10.1109/TIE.2015.2497251.

[3] J.-W. Chui and S.-K. Sui, "New current control concept-minimum time current control in the three-phase PWM converter," *IEEE Transactions on Power Electronics*, vol. 12, no. 1, pp. 124–131, Jan. 1997, doi: 10.1109/63.554177.

[4] F. Niu, K. Li, and Y. Wang, "Direct Torque Control for Permanent-Magnet Synchronous Machines Based on Duty Ratio Modulation," *IEEE Transactions on Industrial Electronics*, vol. 62, no. 10, pp. 6160–6170, Oct. 2015, doi: 10.1109/TIE.2015.2426678.

[5] P. Karamanakos and T. Geyer, "Guidelines for the Design of Finite Control Set Model Predictive Controllers," *IEEE Trans. Power Electron.*, vol. 35, no. 7, pp. 7434–7450, Jul. 2020, doi: 10.1109/TPEL.2019.2954357.

[6] E. Jung, H.-J. Lee, and S.-K. Sul, "FPGA-based motion controller with a high bandwidth current regulator," in *2008 IEEE Power Electronics Specialists Conference*, Jun. 2008, pp. 3043–3047. doi: 10.1109/PESC.2008.4592416.

[7] T. Noguchi, "A New Quick-Response and High-Efficiency Control Strategy of an Induction Motor," *IEEE Transactions on Industry Applications*, vol. IA-22, no. 5, pp. 820–827, Sep. 1986, doi: 10.1109/TIA.1986.4504799.

[8] D. Casadei, F. Profumo, G. Serra, and A. Tani, "FOC and DTC: two viable schemes for induction motors torque control," *IEEE Transactions on Power Electronics*, vol. 17, no. 5, pp. 779–787, Sep. 2002, doi: 10.1109/TPEL.2002.802183.

[9] F. Niu, B. Wang, A. S. Babel, K. Li, and E. G. Strangas, "Comparative Evaluation of Direct Torque Control Strategies for Permanent Magnet Synchronous Machines," *IEEE Transactions on Power Electronics*, vol. 31, no. 2, pp. 1408–1424, Feb. 2016, doi: 10.1109/TPEL.2015.2421321.

[10] S. Lee, C. Hwang, J. Shim, and J. Ha, "A Control Method of Servo Motor Drives for Fast Dynamic Response and Low Torque Ripple," in *2022 IEEE Energy Conversion Congress and Exposition (ECCE)*, Oct. 2022, pp. 01–05. doi: 10.1109/ECCE50734.2022.9947638.

[11] J. Rodriguez *et al.*, "Latest Advances of Model Predictive Control in Electrical Drives—Part II: Applications and Benchmarking With Classical Control Methods," *IEEE Transactions on Power Electronics*, vol. 37, no. 5, pp. 5047–5061, May 2022, doi: 10.1109/TPEL.2021.3121589.

[12] J. Rodriguez *et al.*, "Latest Advances of Model Predictive Control in Electrical Drives—Part I: Basic Concepts and Advanced Strategies," *IEEE Transactions on Power Electronics*, vol. 37, no. 4, pp. 3927–3942, Apr. 2022, doi: 10.1109/TPEL.2021.3121532.

[13] M. Preindl and S. Bolognani, "Model Predictive Direct Speed Control with Finite Control Set of PMSM Drive Systems," *IEEE Transactions on Power Electronics*, vol. 28, no. 2, pp. 1007–1015, Feb. 2013, doi: 10.1109/TPEL.2012.2204277.

[14] N. S. Nise, "Control Systems Engineering, 8th Edition," *Wiley*, Feb. 2019.